

# Rovibrational spectra of DCF<sub>3</sub> in the 2000 cm<sup>-1</sup> region: A high-resolution study of the $\nu_5 = 2$ and $\nu_2 = \nu_5 = 1$ levels



Adina Ceausu-Velcescu<sup>a,\*</sup>, Petr Pracna<sup>b</sup>, Adriana Predoi-Cross<sup>c</sup>

<sup>a</sup> Univ. Perpignan Via Domitia, Laboratoire de Mathématiques et Physique, EA 4217, F-66860 Perpignan, France

<sup>b</sup> J. Heyrovský Institute of Physical Chemistry, v.v.i., Academy of Sciences of the Czech Republic, Dolejškova 3, 18223 Prague, Czech Republic

<sup>c</sup> University of Lethbridge, Department of Physics and Astronomy, 4401 University Drive, Lethbridge, AB T1 K 3M4, Canada

## ARTICLE INFO

### Article history:

Received 26 June 2014

In revised form 28 August 2014

Available online 18 September 2014

### Keywords:

Deuterated fluorofrom

Overtone bands

Combination bands

Reduced Hamiltonian

## ABSTRACT

The high-resolution infrared spectrum of DCF<sub>3</sub> was investigated in the 2000 cm<sup>-1</sup> region, with the aim of assigning and analyzing the overtone bands  $2\nu_5$  ( $A_1 + E$ ), as well as the combination band  $\nu_2 + \nu_5$  ( $E$ ). The present paper reports on the first high-resolution study of the  $\nu_2 = \nu_5 = 1$  and  $\nu_5 = 2$  levels, through the analysis of the combination  $\nu_2 + \nu_5$  and the overtone  $2\nu_5^{\pm 2}$  bands respectively. This analysis can be thought of as a necessary step toward the reinvestigation of the complicated vibrational pattern in the CD stretching fundamental region.

© 2014 Elsevier Inc. All rights reserved.

## 1. Introduction

The HCF<sub>3</sub> molecule (fluorofrom or trifluoromethane) and its deuterated isotopologue DCF<sub>3</sub> are oblate symmetric-top molecules ( $I_A = I_B < I_C$ ), belonging to the point group  $C_{3v}$ . These molecules have six fundamental vibrations, labeled  $\nu_1$  to  $\nu_6$ . Three of them,  $\nu_1$ ,  $\nu_2$ , and  $\nu_3$ , are nondegenerate vibrations of  $A_1$  symmetry; the three remaining vibrations  $\nu_4$ ,  $\nu_5$ , and  $\nu_6$  are doubly degenerate vibrations of  $E$  symmetry.

This paper represents a further contribution to the systematic investigation of overtone and combination vibrational levels of deuterated fluorofrom, DCF<sub>3</sub>, with the ultimate goal of reaching the region of the highest fundamental level  $\nu_1 = 1$  corresponding to the C–D stretching vibration [1]. We believe this region needs to be reanalyzed. The studies of the deuterated isotopologue [2–8] comprise significantly more overtone and combination levels than studies of the HCF<sub>3</sub> molecule because two of the fundamental vibrational energies of DCF<sub>3</sub> are significantly lower than in the parent species. Only a few overtone/combination levels have been studied for HCF<sub>3</sub> [9–11].

An overview of the vibrational levels studied so far in DCF<sub>3</sub> is shown in Fig. 1. With the exception of the  $\nu_2 = 1$ ,  $\nu_3 = 1$ ,  $\nu_2 = \nu_3 = 1$ , and  $\nu_2 = \nu_6 = 1$  levels, which were analyzed as isolated

ones, all other studies had to take into account various anharmonic and rovibrational resonant interactions. A detailed knowledge of these interactions allowed modeling analogous interaction schemes in higher excited vibrational states and led to their quantitative description despite the fact that some of the levels in these complex polyads were ‘dark’ states.

This approach was first applied in the analysis of the  $\nu_3 = \nu_5 = 1$  combination level [7], which needed to have the interactions in the cluster together with the  $\nu_3 = 2$ ,  $\nu_6 = 1$  and  $\nu_4 = \nu_6 = 1$  levels included explicitly. We could extrapolate these interactions from the ‘parent’ systems [3,5]. We are using a similar approach in the present study of the  $\nu_5 = 2$  overtone and  $\nu_2 = \nu_5 = 1$  combination levels, for which the parent system is the  $\nu_5 = 1/\nu_6 = 2$  dyad. Indeed the  $\nu_5 = 2/\nu_5 = 1$ ,  $\nu_6 = 2$  dyad is generated by adding a  $\nu_5$  vibrational quantum to the  $\nu_5 = 1/\nu_6 = 2$  system, whereas the  $\nu_2 = \nu_5 = 1/\nu_2 = 1$ ,  $\nu_6 = 2$  dyad is obtained from the same parent system by adding a  $\nu_2$  vibrational quantum. In the latter case, the  $\nu_2$  quantum corresponds to a nondegenerate vibration, and hence the upper dyad has essentially the same structure as the parent system.

For the  $\nu_5 = 2$  overtone level, however, the addition of the quantum of a degenerate vibration creates a completely different interaction pattern. It consists of an  $A_1 + E$  system of sublevels of  $\nu_5 = 2$  and an  $A_1 + A_2 + 2E$  system of sublevels of  $\nu_5 = 1$ ,  $\nu_6 = 2$  (see later in Section 5). We were able to extrapolate the interactions from the parent system and achieve a quantitative description of the  $\nu_5 = 2$  level in spite of the perturbing  $\nu_5 = 1$ ,  $\nu_6 = 2$  combination level being a completely dark state.

\* Corresponding author at: Université de Perpignan Via Domitia, Laboratoire de Mathématiques et Physique, 52 Avenue Paul Alduy, F-66860 Perpignan France. Fax: +33 4 68 66 22 34.

E-mail address: [adina@univ-perp.fr](mailto:adina@univ-perp.fr) (A. Ceausu-Velcescu).

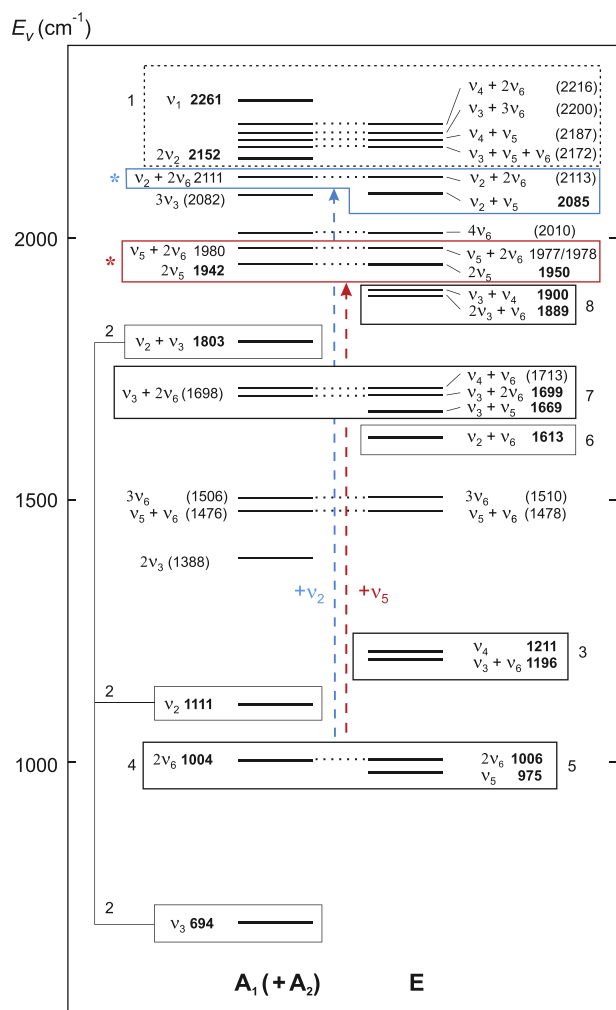


**Fig. 1.** Diagram of vibrational levels of  $\text{DCF}_3$  between 500 and  $2500\text{ cm}^{-1}$ , separated to nondegenerate ( $A_1$ ,  $A_2$ ) and degenerate ( $E$ ) levels. The levels analyzed so far are highlighted with bold lines and fonts. The energies of overtone and combination levels given in parentheses are estimated by including anharmonic corrections either from experiment, or from *ab initio* calculations. Those levels which have to be treated as polyads are enclosed in bold boxes. Reference numbers to the recently accomplished analyses [2–8] are also shown in the figure.

The two clusters of levels studied here could be treated as independent polyads as their mutual couplings are weak and thus could be neglected.

## 2. Experimental details

Two high-resolution FTIR spectra were used in this work; one from the region  $1850\text{--}2040\text{ cm}^{-1}$  (spectrum I), used for assignments of the  $2\nu_5^{\pm 2}$  band, and another one from the region  $2020\text{--}2500\text{ cm}^{-1}$  (spectrum II), adopted for assignments of the  $\nu_2 + \nu_5$  band. Both spectra were recorded at the Canadian Light Source in Saskatoon with a Bruker IFS 125HR spectrometer.

A third spectrum, recorded in Wuppertal with a Bruker IFS 120HR spectrometer, already used in Refs. [2,6,7], referred there as #1611, was used in this work for calibration purposes. Spectra I and II were thus calibrated by well developed, isolated lines of  $\text{DCF}_3$  from spectrum III, in order to achieve the best wavenumber consistency of the three spectra. Wavenumber precision and accuracy of spectra I and II were estimated to be  $1 \times 10^{-4}$  and  $3 \times 10^{-4}\text{ cm}^{-1}$ , respectively.

**Table 1**  
Experimental details of Fourier transform spectra used in this study.

Spectrum	I	II	III
Range ( $\text{cm}^{-1}$ )	1850–2040	2020–2500	1240–2050
Detector	Cu:Ge	In:Sb	MCT800
Beamsplitter	KBr	KBr	KBr
No. of scans	200	200	341
Resolution <sup>a</sup> ( $\text{cm}^{-1}$ )	0.002	0.002	0.0024
Path length (m)	16	16	9.6
Pressure (Pa)	158.7	158.7	250
Temperature (K)	296	296	293

<sup>a</sup> The resolution of the Bruker FTS was calculated as  $1/\text{MOPD}$ , where MOPD is maximum optical path difference.

The details of experimental conditions of these spectra are summarized in Table 1.

## 3. Description of the spectrum and assignments

### 3.1. The $2\nu_5$ overtone bands

From the  $2\nu_5$  overtone bands, only the perpendicular component  $2\nu_5^{\pm 2}$  could be observed and assigned in the available spectra. This band, clearly visible on the spectrum around  $1950\text{ cm}^{-1}$  (Fig. 2a), is quite well separated from the  $\nu_3 + \nu_4/2\nu_3 + \nu_6$  system, near  $1900\text{ cm}^{-1}$  [8]. For low-to-intermediate  $K$  values, the  $Q$ -branches of this perpendicular band are equally spaced by about  $0.27\text{ cm}^{-1}$ , which roughly corresponds to  $2(C - B + 2C'_2)$ , i.e. the separation between adjacent  $Q$ -branches of an unperturbed perpendicular band. These  $Q$ -branches are located in a relatively narrow region around the band center, with an  ${}^rQ_0$  branch near  $1950.33\text{ cm}^{-1}$  (Fig. 3).

On the lower wavenumbers side of the spectrum, the strong  ${}^pP_K$  lines, shown in Fig. 4a, form nice progressions of the type ( ${}^pP_K(J)$ ,  ${}^pP_{K-3}(J+1)$ , ...). Prominent progressions of lines ( ${}^rR_K(J)$ ,  ${}^rR_{K-3}(J+1)$ , ...) are then visible on the higher wavenumbers side, as shown in Fig. 4b. The lines of the former progressions become more and more closely spaced with increasing  $J$ . On the contrary, the lines of the latter ( $\Delta K = +1$ ) progressions become more and more spread with increasing  $J$ , and prominent clusters of lines ( ${}^rR_K(J)$ ,  ${}^rR_{K+2}(J-1)$ , ...) occur near  $1970\text{ cm}^{-1}$  and above. Two such adjacent clusters are separated by a distance which is roughly equal to  $B$ , each cluster containing only lines with either even or odd  $K$  values. Lines of these clusters clearly show intensity alternation due to nuclear spin statistics, as illustrated in Fig. 5.

In both  ${}^pP_K$  and  ${}^rR_K$  cases,  $K$  and  $J$  assignments were easily achieved by looking for first lines (i.e. lines having  $J = K$ ). The  $J/K$  assignments of the  ${}^pP_K$  and  ${}^rR_K$  branches were then checked against the corresponding  ${}^pQ_K/{}^rQ_K$  branches, by lower state combination differences (LSCD),<sup>1</sup> using the Loomis–Wood for Windows program [12]. A total of 2199 transitions belonging to the  $2\nu_5$  band ( $-42 \leq K \cdot \Delta K \leq 42$ ,  $J_{\text{max}} = 56$ ), assigned from spectrum I, were used in the least-squares calculations.

### 3.2. The $\nu_2 + \nu_5$ combination band

The  $\nu_2 + \nu_5$  band, centered at  $2085.04\text{ cm}^{-1}$ , has the appearance of a textbook perpendicular band, roughly extending from about  $2050$  to  $2100\text{ cm}^{-1}$  (Fig. 2b). The  $Q$ -branches of this combination band are quite regularly spaced by about  $-0.55\text{ cm}^{-1}$ , which corresponds to the value of  $2(C - B - C'_2)$ . The  ${}^pQ_K/{}^rQ_K$  branches

<sup>1</sup> The LSCD checking of assignments is, however, not possible for the  ${}^pP_K(J = K)$  lines, which terminate on the  $(K - 1, J = K - 1)$  'lonely' levels and hence have no  ${}^pQ_K(J)$  counterpart.

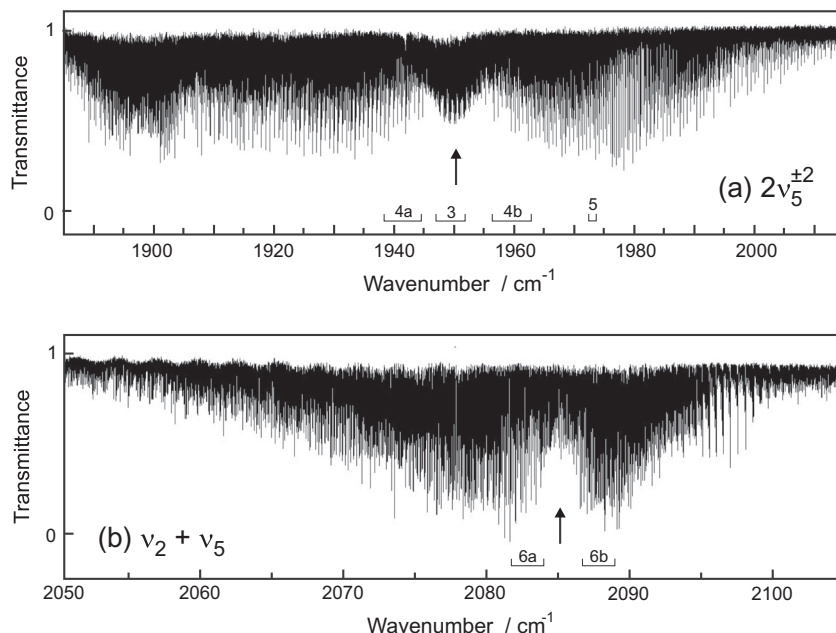


**Fig. 2.** Overview of the  $2\nu_5$  (a) and  $\nu_2 + \nu_5$  (b) bands of  $\text{DCF}_3$ . The intervals below the spectrum refer to the sections shown in further figures with the corresponding figure numbers. The arrows point to band origins, more precisely to the heads of the  ${}^rQ_0$  branches. Experimental conditions: pressure 158.7 Pa, path length 16 m, resolution (1/MOPD)  $0.002 \text{ cm}^{-1}$ .

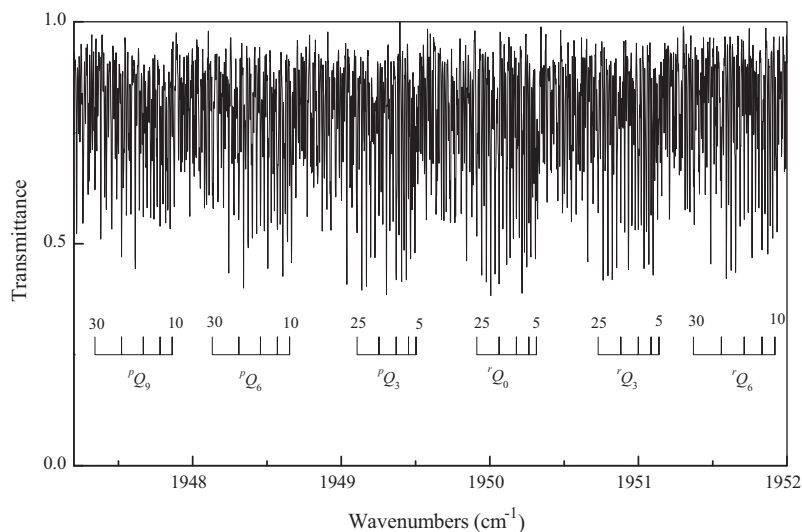


**Fig. 3.** Detail of the spectrum in the region of the  ${}^pQ_9$  to  ${}^rQ_6$  branches of the  $2\nu_5^{\pm 2}$  band with assignment combs indicating some of the values of  $j$  with steps of  $j = 5n$ , for the  ${}^xQ_K$  branches ( $x = p$  or  $r$ ) with  $K = 3p$ . Experimental conditions as for Fig. 2.

are frequently overlapped by lines of the  $P/R$  branches and hidden among them.

On the lower wavenumber side of the spectrum, the clearest patterns are the series of  ${}^pP_K(J = K)$ ,  ${}^pP_K(J = K + 1)$ ,  ${}^pP_K(J = K + 2)$ , ... lines, shown in Fig. 6a ( $K = 1, 2, \dots$  within such a series). In the higher wavenumber region, the series of  ${}^rR_K(J = K)$ ,  ${}^rR_K(J = K + 1)$ , ...  ${}^rR_K(J = K + n)$  lines are well-resolved up to  $n = 12$  (Fig. 6b), then progressively collapse to clusters of overlapped lines for  $n \leq 21$  and become resolved again for higher  $J$ -values.

The  ${}^pP_K/{}^rR_K$  series, from which the assignments were started, were as usual checked by LSCD [12]. For this purpose, only the  ${}^pQ_K/{}^rQ_K$  corresponding lines could be used, because the  ${}^pR_K/{}^pP_K$  transitions have vanishing intensities. A total of 2461 transitions belonging to the  $\nu_2 + \nu_5$  band ( $-42 \leq K \cdot \Delta K \leq 42$ ,  $J_{\max} = 60$ ),

assigned from spectrum II, were used in the least-squares calculations.

#### 4. Theoretical model

The general notation  $\mathbf{H}_{mn}$ , where  $m$  is the total power of vibrational operators and  $n$  the total power of rotational operators, has been used throughout the paper. Such a  $\mathbf{H}_{mn}$  term in the development of the rovibrational Hamiltonian is of order  $i = m + n - 2$  in the Amat and Nielsen classification [13].

The matrix elements of the effective Hamiltonians for the individual vibrational states  $\nu_5 = 2 (A_1 + E)$  and  $\nu_2 = \nu_5 = 1 (E)$ , up to fifth order, are given in the Appendix A.

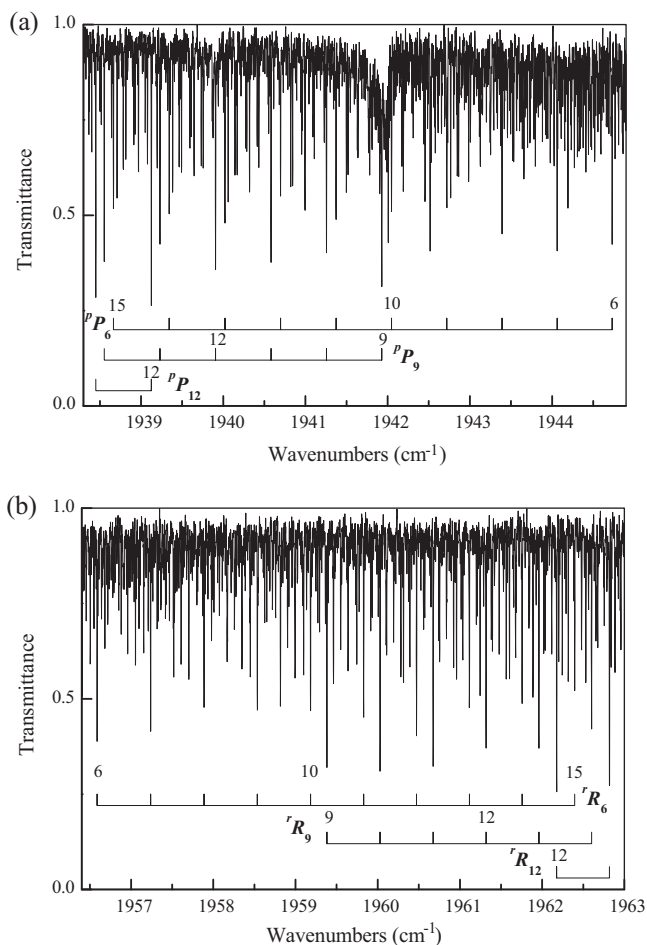


**Fig. 4.** (a) Detail of the spectrum in the region of the  ${}^pP_K$  lines of the  $2\nu_5^{-2}$  band, with assignment combs indicating some of the values of  $J$  for the  ${}^pP_6$ ,  ${}^pP_9$ , and  ${}^pP_{12}$  series. (b) Detail of the spectrum in the region of the  ${}^rR_K$  lines of the  $2\nu_5^{-2}$  band, with assignment combs indicating some of the values of  $J$  for the  ${}^rR_6$ ,  ${}^rR_9$ , and  ${}^rR_{12}$  series. Experimental conditions as for Fig. 2.

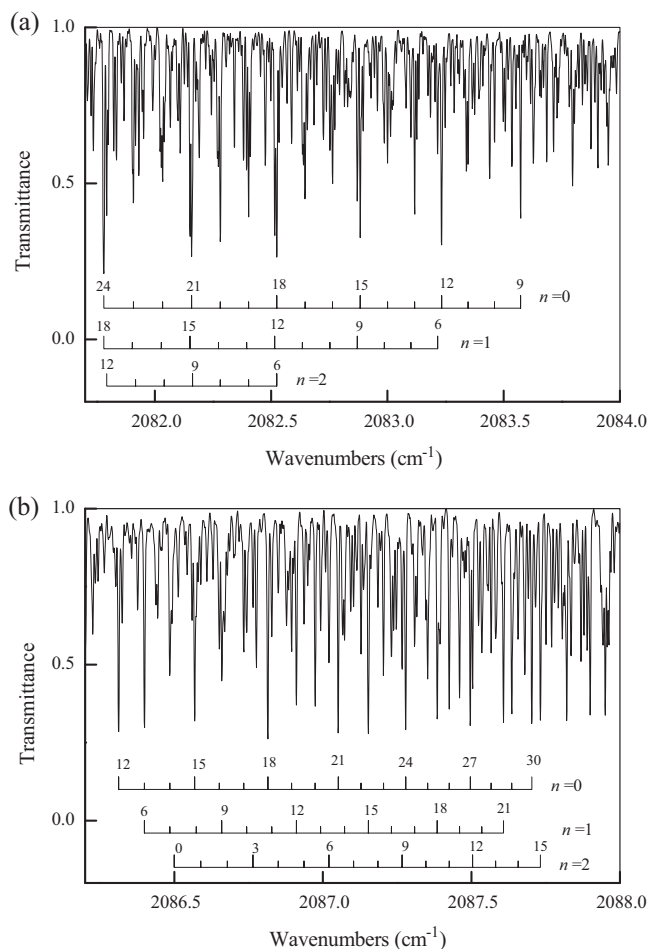


**Fig. 6.** (a) Detail of the spectrum in the region of the  ${}^pP_K$  lines of the  $\nu_2 + \nu_5$  band, showing  ${}^pP_K(J = K + n)$  ( $K = 1, 2, \dots$ ) series for  $n = 0, 1$ , and  $2$ , with some of the  $K$  assignments indicated. (b) Detail of the spectrum in the region of the  ${}^rR_K$  lines of the  $\nu_2 + \nu_5$  band, showing  ${}^rR_K(J = K + n)$  ( $K = 0, 1, 2, \dots$ ) series for  $n = 0, 1$ , and  $2$ , with some of the  $K$  assignments indicated. Experimental conditions as for Fig. 2.

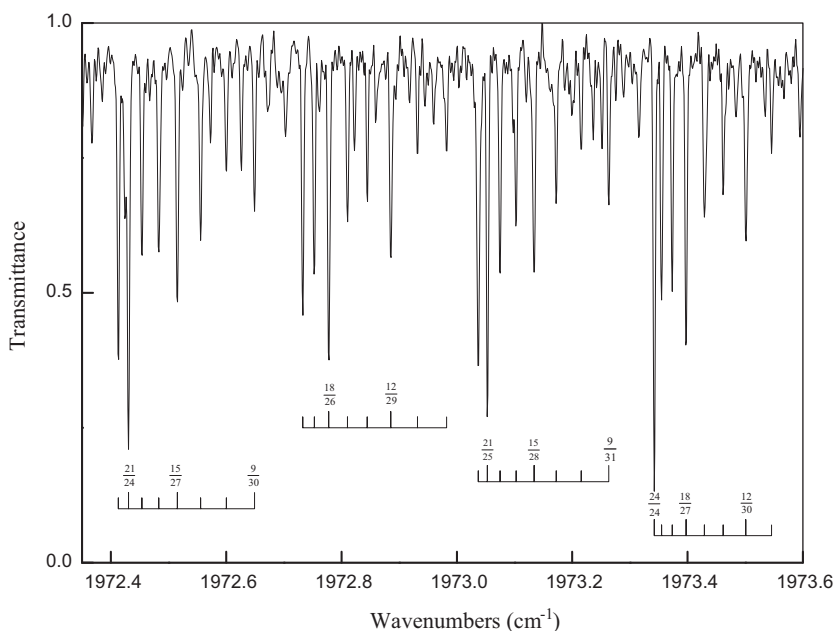


**Fig. 5.** Detail of the spectrum in the region of the  ${}^rR_K$  lines of the  $2\nu_5^{-2}$  band, showing some prominent clusters of lines  ${}^rR_K(J)$ ,  ${}^rR_{K+2}(J - 1)$ , ... Assignments combs indicate some of the  $J$  values. Experimental conditions as for Fig. 2.

**Table 2**  
Molecular parameters of DCF<sub>3</sub> (in cm<sup>-1</sup>) in the  $\nu_5 = 2$  and  $\nu_5 = 1$ ,  $\nu_6 = 2$  vibrational levels.

Parameter	$\nu_5 = 2, l_5 = 0$	$\nu_5 = 2, l_5 = \mp 2$	$\nu_5 = 1, l_5 = \pm 1, \nu_6 = 2, l_6 = 0$	$\nu_5 = 1, l_5 = \mp 1, \nu_6 = 2, l_6 = \pm 2$	$\nu_5 = 1, l_5 = \pm 1, \nu_6 = 2, l_6 = \pm 2$
<i>E</i>	1942.011406	1950.075735(23)	1977.368531	1977.892039	1980.692039
<i>B</i>	0.3303539(48)	0.33029305(19)	0.3307055(54)	0.33104845(76)	0.330057(15)
<i>C</i>	0.1893951(19)	0.189232300(96)	0.1883245(37)	0.18853698	0.18853698
<i>D<sub>J</sub></i> × 10 <sup>7</sup>	3.198603 <sup>a</sup>	3.24242(64)	3.198603 <sup>a</sup>	3.198603 <sup>a</sup>	3.198603 <sup>a</sup>
<i>D<sub>JK</sub></i> × 10 <sup>7</sup>	−4.892648 <sup>a</sup>	−4.7666(19)	−4.892648 <sup>a</sup>	−4.892648 <sup>a</sup>	−4.892648 <sup>a</sup>
<i>D<sub>K</sub></i> × 10 <sup>7</sup>	2.178876 <sup>a</sup>	2.0707(15)	2.178876 <sup>a</sup>	2.178876 <sup>a</sup>	2.178876 <sup>a</sup>
<i>H<sub>J</sub></i> × 10 <sup>13</sup>	4.74505 <sup>a</sup>	4.74505 <sup>a</sup>	4.74505 <sup>a</sup>	4.74505 <sup>a</sup>	4.74505 <sup>a</sup>
<i>H<sub>JK</sub></i> × 10 <sup>12</sup>	−2.006503 <sup>a</sup>	−2.006503 <sup>a</sup>	−2.006503 <sup>a</sup>	−2.006503 <sup>a</sup>	−2.006503 <sup>a</sup>
<i>H<sub>KJ</sub></i> × 10 <sup>12</sup>	2.599420 <sup>a</sup>	2.599420 <sup>a</sup>	2.599420 <sup>a</sup>	2.599420 <sup>a</sup>	2.599420 <sup>a</sup>
<i>H<sub>K</sub></i> × 10 <sup>12</sup>	−1.04962 <sup>a</sup>	−1.04962 <sup>a</sup>	−1.04962 <sup>a</sup>	−1.04962 <sup>a</sup>	−1.04962 <sup>a</sup>
<i>Cζ</i>		0.13825993(54)	0.138488593 <sup>b</sup>	−0.421595353	−0.1446174
<i>η<sub>J</sub></i> × 10 <sup>6</sup>		1.7363(25)	1.64062 <sup>b</sup>	−3.89062	−0.609381
<i>η<sub>K</sub></i> × 10 <sup>6</sup>		−1.7088(32)	−1.56914 <sup>b</sup>	3.36554	0.2272599
<i>τ<sub>J</sub></i> × 10 <sup>10</sup>		−0.1072 <sup>b</sup>	−0.1072 <sup>b</sup>	0.1072	−0.1072
<i>τ<sub>JK</sub></i> × 10 <sup>10</sup>		1.982(30)	2.1183 <sup>b</sup>	−2.1183	2.1183
<i>τ<sub>K</sub></i> × 10 <sup>10</sup>		−2.254(28)	−2.3431 <sup>b</sup>	2.3431	−2.3431
<i>q<sub>22</sub></i> × 10 <sup>4</sup>	−0.2029(18)	−0.19817 <sup>b</sup>	−2.64097 <sup>b</sup>		
<i>f<sub>22</sub><sup>J</sup></i> × 10 <sup>9</sup>	0.9095 <sup>b</sup>	0.9095 <sup>b</sup>	1.0127 <sup>b</sup>		
<i>f<sub>22</sub><sup>K</sup></i> × 10 <sup>9</sup>			−1.007 <sup>b</sup>		
<i>q<sub>12</sub></i> × 10 <sup>5</sup>	3.8807(71)				
<i>f<sub>42</sub></i> × 10 <sup>9</sup>		−0.5566 <sup>b</sup>			
<i>d<sub>t</sub></i> × 10 <sup>6</sup>		0.280(17)			
<i>d<sub>t</sub><sup>l</sup></i> × 10 <sup>11</sup>		0.2601 <sup>b</sup>			
NZW data	0	2199	0	0	0
Range of <i>J/K</i>		56/42			
Standard deviation × 10 <sup>4</sup>		3.99			

Numbers in parentheses are standard deviations in units of the last digit quoted.

NZW = non-zero weighted.

<sup>a</sup> Constrained to the corresponding ground state values, quoted in Ref. [4].

<sup>b</sup> Constrained to the corresponding  $\nu_5 = 1$  or  $\nu_6 = 2$  values, quoted in Ref. [5].

For the  $\nu_5 = 2$  level, an additional part of the Hamiltonian that describes its interactions with the ( $\nu_5 = 1, \nu_6 = 2$ ) level has been considered. This interaction part includes a Fermi interaction ( $\Delta k = 0, \Delta l = \sum_t \Delta l_t = \pm 3$ ), a higher-order Coriolis resonance ( $\Delta k = \Delta l = \pm 1$ ), a higher-order  $\alpha$ -resonance ( $\Delta k = \mp 2, \Delta l = \pm 1$ ), and also a higher-order anharmonic resonance ( $\Delta k = 0, \Delta l = \pm 3$ ). The corresponding matrix elements are equally given in Appendix A.

For the  $\nu_2 = \nu_5 = 1$  level, the interaction scheme, which is very similar to that of the lower system  $\nu_5 = 1/\nu_6 = 2$  [5], comprises an anharmonic Fermi interaction, a higher-order Coriolis resonance and a higher-order  $\alpha$  resonance with the  $\nu_2 = 1, \nu_6 = 2$  levels.

The ground state parameters, kept fixed in both least-squares procedures, are those quoted in Ref. [4], which are the most accurate experimental values presently available for this molecule. The resulting parameters for excited states are listed in Tables 2–4.

## 5. Results and discussion

The  $2\nu_5^{\mp 2}$  perpendicular band shows an important ‘local’ perturbation due to a ( $\Delta k = \mp 2, \Delta l = \pm 1$ ) interaction with the ( $\nu_5^l = 1^{-1}, \nu_6^l = 2^{-2}$ ) ‘dark’ sublevel.

The data belonging to the  $2\nu_5^{\mp 2}$  band could nevertheless be fitted in a first step by a simple model of an isolated overtone level. Results were, however, improved by including the Coriolis and  $\alpha$ -interactions with the ( $\nu_5 = 1, \nu_6 = 2$ ) ‘dark’ level.

The ( $\nu_5 = 1, \nu_6 = 2$ ) vibrational level includes the following sublevels:

- ( $\nu_5 = 1, l_5 = \pm 1, \nu_6 = 2, l_6 = 0$ ) (*E* symmetry).
- ( $\nu_5 = 1, l_5 = \mp 1, \nu_6 = 2, l_6 = \pm 2$ ) (*E* symmetry).
- ( $\nu_5 = 1, l_5 = \pm 1, \nu_6 = 2, l_6 = \pm 2$ ) (*A*<sub>1</sub> + *A*<sub>2</sub> symmetry).

This new kind of vibrational level and its specific intra- and inter-vibrational interactions (see Fig. 7) had to be introduced explicitly in the code that generates the Z-matrix [14].

The refinement of the  $q_{12}$  ( $\Delta k = \mp 1, \Delta l = \pm 2$ ) interaction parameter in the  $\nu_5 = 2$  level was also found to greatly improve the quality of the fit. The ( $\nu_5 = 2, l_5 = 0, K$ )/( $\nu_5 = 2, l_5 = +2, K - 1$ ) levels show indeed a large variety of crossings, occurring for  $K = 21$  to 30 (Fig. 8); the *J*-value for which such crossings occur increases slightly with *K*. The analysis demonstrated, as in the case of the  $\nu_{10} = 2$  state of CF<sub>3</sub>CCH [15], that the  $\eta_J, \eta_K, q_{12}$ , and *d<sub>t</sub>* parameters can be refined simultaneously for an overtone state without correlation problems. The *s* parameter in the contact transformation was thus specified by the constraint  $\tilde{q}_{12}^l = 0$  (*L*-reduction).

As in the case of the  $\nu_5 = 1$  fundamental level, the *D*-reduction had to be avoided, due to the accidental smallness of the  $q_{22}$  *l*-type interaction parameter.

Besides these intra- and inter-vibrational interactions, a perturbation was observed in the  $2\nu_5^{\pm 2}$  subband, for  $K = 28$  and above. As this perturbation is clearly effective even for the lowest *J*-values, it must be of the anharmonic type. An anharmonic resonance  $2\nu_5^{\mp 2}/\nu_5^{\pm 1} + 2\nu_6^0$  is possible through a **H**<sub>50</sub> third-order vibrational operator. From the above-mentioned pairs of levels, the  $2\nu_5^{\pm 2}$  and  $\nu_5^{\pm 1} + 2\nu_6^0$  levels diverge from each other and no crossing occurs. At the same time, the  $2\nu_5^{\pm 2}$  and  $\nu_5^{\pm 1} + 2\nu_6^0$  levels come closer together with growing *K* (see Fig. 8). This anharmonic interaction was found to be significant in the present analysis and was thus included in the interaction Hamiltonian.

There is, however, one local ( $\Delta k = \sum_t \Delta l_t = \pm 1$ ) interaction between the ( $\nu_5^l = 2^{-2}; J, K$ ) and ( $\nu_5^l = 1^{+1}, \nu_6^l = 2^{-2}; J, K + 1$ ) levels, mainly affecting the 16/17 and 17/18 pairs of levels, which has not been included in the model. Such an interaction takes place through a **H**<sub>51</sub> higher-order Coriolis operator; crossing occurs

**Table 3**  
Molecular parameters of DCF<sub>3</sub> (in cm<sup>-1</sup>) in the  $\nu_2 = \nu_5 = 1$  vibrational level and comparison with those of the vibrational ground state and the two corresponding fundamental levels.

Parameter	Ground state <sup>a</sup>	$\nu_2 = 1^b$	$\nu_5 = 1^c$	$\nu_2 = \nu_5 = 1$
<i>E</i>		1111.182898	975.50827184	2085.041819(17)
<i>B</i>	0.3309331091	0.329081566	0.330621982	0.32864068(25)
<i>C</i>	0.18924413	0.18877579	0.189243975	0.18876413(12)
<i>D<sub>J</sub></i> × 10 <sup>7</sup>	3.198603	3.134004	3.21823	3.05528(73)
<i>D<sub>JK</sub></i> × 10 <sup>7</sup>	-4.89265	-4.093276	-4.80395	-3.6520(22)
<i>D<sub>K</sub></i> × 10 <sup>7</sup>	2.178876	1.46381	2.09656	1.1122(21)
<i>H<sub>J</sub></i> × 10 <sup>13</sup>	4.7451	4.1162	4.437	4.437 <sup>d</sup>
<i>H<sub>JK</sub></i> × 10 <sup>12</sup>	-2.0065	1.2315	-1.972	4.309(51)
<i>H<sub>KJ</sub></i> × 10 <sup>12</sup>	2.5994	-6.3400	3.371	-11.81(12)
<i>H<sub>K</sub></i> × 10 <sup>12</sup>	-1.0496	5.5705	-2.262	6.427(91)
<i>C<sub>ξ</sub></i>			0.138488953	0.13783723(76)
<i>η<sub>J</sub></i> × 10 <sup>6</sup>			1.64062	2.2602(41)
<i>η<sub>K</sub></i> × 10 <sup>6</sup>			-1.56914	-2.1999(56)
<i>τ<sub>J</sub></i> × 10 <sup>10</sup>			-0.1072	-0.1072 <sup>d</sup>
<i>τ<sub>JK</sub></i> × 10 <sup>10</sup>			2.1183	2.912(27)
<i>τ<sub>K</sub></i> × 10 <sup>10</sup>			-2.3431	-3.407(22)
<i>q<sub>22</sub></i> × 10 <sup>4</sup>			-0.198170	0.55469(47)
<i>f<sub>22</sub><sup>J</sup></i> × 10 <sup>9</sup>			0.9095	-1.992(34)
<i>f<sub>42</sub></i> × 10 <sup>10</sup>			-5.57	16.50(47)
<i>d<sub>t</sub></i> × 10 <sup>7</sup>			4.1804	3.52(11)
<i>d<sub>t</sub><sup>J</sup></i> × 10 <sup>12</sup>			2.6011	2.6011 <sup>d</sup>
<i>h<sub>3</sub></i> × 10 <sup>14</sup>	-7.4939		-7.4939	-7.4939 <sup>d</sup>
<i>h<sub>3</sub><sup>J</sup></i> × 10 <sup>19</sup>	4.77		4.77	4.77 <sup>d</sup>
NZW data				2461
Range of <i>J/K</i>				58/41
Standard deviation × 10 <sup>4</sup>				2.53

Numbers in parentheses are standard deviations in units of the last digit quoted.

<sup>a</sup> Ref. [4].

<sup>b</sup> Ref. [2].

<sup>c</sup> Ref. [5].

<sup>d</sup> Fixed to the corresponding  $\nu_5 = 1$  value, quoted in Ref. [5].

**Table 4**

Inter-vibrational interaction parameters for the  $\nu_5 = 2/\nu_5 = 1$ ,  $\nu_6 = 2$  and  $\nu_2 = \nu_5 = 1/\nu_2 = 1$ ,  $\nu_6 = 2$  level systems of DCF<sub>3</sub> (in cm<sup>-1</sup>).

Interaction	Parameter	Value		
		$\nu_5 = 1/\nu_6 = 2^a$	$\nu_5 = 2/\nu_5 = 1$ , $\nu_6 = 2$	$\nu_2 = \nu_5 = 1/\nu_2 = 1$ , $\nu_6 = 2$
Coriolis ( $\Delta k = \Sigma_t \Delta l_t = \pm 1$ )	$f_{31}^{xa} \times 10^3$	-3.734(33)	-1.138(50)	-1.289(80)
	$f_{33}^{xaJ} \times 10^7$	-3.55(14)	-3.55 <sup>b</sup>	-3.55 <sup>b</sup>
	$f_{33}^{xa,K} \times 10^6$	5.345	5.345 <sup>b</sup>	5.345 <sup>b</sup>
Coriolis ( $\Delta k = \Sigma_t \Delta l_t = \pm 1$ )	$f_{31}^{xb} \times 10^3$	-7.298(30)	-7.02(10)	-7.99(21)
	$f_{33}^{xbJ} \times 10^7$	-8.18(14)	-8.18 <sup>b</sup>	-8.18 <sup>b</sup>
	$f_{33}^{xb,K} \times 10^6$	1.044	1.044 <sup>b</sup>	1.044 <sup>b</sup>
$\alpha$ -Resonance ( $\Delta k = \pm 2$ , $\Sigma_t \Delta l_t = \mp 1$ )	$f_{32}^{xxa} \times 10^5$	-3.28(39)	6.34(51)	-26.20(15)
$\alpha$ -Resonance ( $\Delta k = \pm 2$ , $\Sigma_t \Delta l_t = \mp 1$ )	$f_{32}^{xxb} \times 10^6$	9.556(24)	8.04(96)	9.556 <sup>b</sup>
Fermi ( $\Delta k = 0$ , $\Sigma_t \Delta l_t = \pm 3$ )	$k_{566}$	-1.442	-1.381 <sup>c</sup>	-1.442 <sup>b</sup>
Fermi ( $\Delta k = 0$ , $\Sigma_t \Delta l_t = \pm 3$ )	$W_{5566}$	-	-0.22465(19)	-

Numbers in parentheses are standard deviations in units of the last digit quoted.

<sup>a</sup> Ref. [5].

<sup>b</sup> Constrained to the  $\nu_5 = 1/\nu_6 = 2$  corresponding value, quoted in Ref. [5].

<sup>c</sup> Constrained to a value obtained in a preliminary fit (see text).

between the ( $\nu_5^2 = 2^{-2}; J, K = 17$ ) and ( $\nu_5^1 = 1^{+1}, \nu_6^2 = 2^{-2}; J, K = 18$ ) levels, near  $J = 45$ . Nevertheless, the  ${}^rX_{15}$  and  ${}^rX_{16}$  transitions ( $X = Q, R$ ) of the  $2\nu_5^{-2}$  subband, affected by this local interaction, were kept in the least-squares calculations with weights proportional to the inverse square of their estimated experimental uncertainties.<sup>2</sup>

<sup>2</sup> Neglecting this interaction did however spoil neither the description of the  $2\nu_5$  band, nor the quality of its parameters.

Now, a few words should be said concerning the Fermi non-resonant interaction due to the  $\mathbf{H}_{30}$  Hamiltonian term (see Appendix A). The Fermi parameter  $k_{566}$ , which is analogous to that introduced for the lower  $\nu_5/2\nu_6$  dyad, was first released, but with  $f_{32}^{xxa}$  and  $f_{32}^{xxb}$  temporarily kept fixed, in order to avoid strong correlations between them. The obtained value,  $k_{566} \approx -1.381$  cm<sup>-1</sup>, is only slightly different from that used in the  $\nu_5/2\nu_6$  system, which is  $-1.442$  cm<sup>-1</sup>. Eventually,  $k_{566}$  was

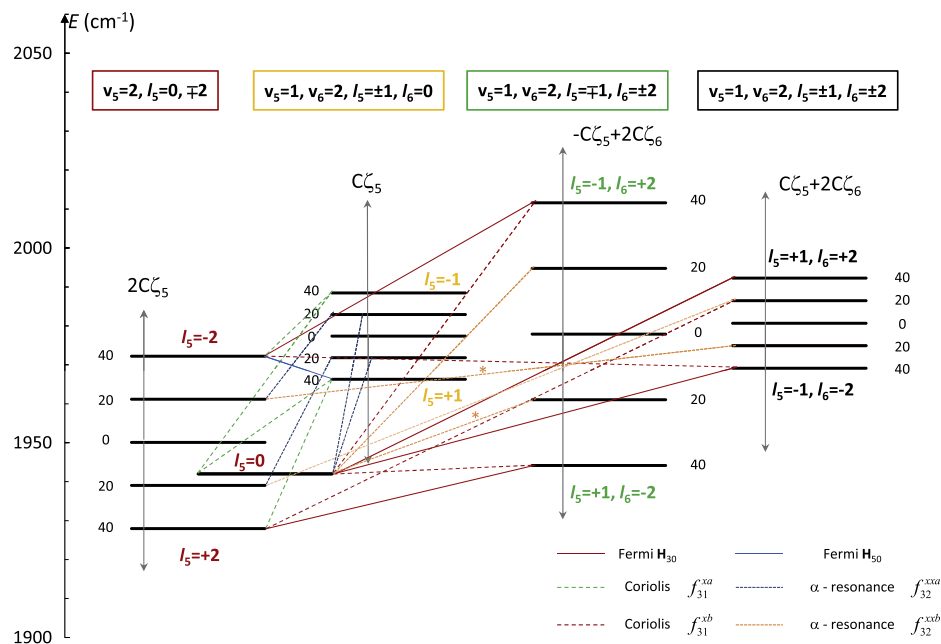


**Fig. 7.** Interaction scheme of the  $l$ -sublevels in the  $\nu_5 = 2/\nu_5 = 1$ ,  $\nu_6 = 2$  system, with the inter-vibrational interactions indicated: Fermi (full lines), Coriolis (dashed lines), and  $\alpha$ -resonances (dotted lines). The energies are approximated as  $E = E_v - 2\sum_l (C_l^x l_x)K$  and drawn only for some selected  $K$  values, in order to illustrate changes of the relative spacing of the  $(\pm l)$  levels with growing  $K$ . The lines representing interactions connect the stacks of  $(K, l)$  levels as a whole, without obeying the particular  $\Delta K$  selection rules for the non-vanishing Hamiltonian matrix elements.

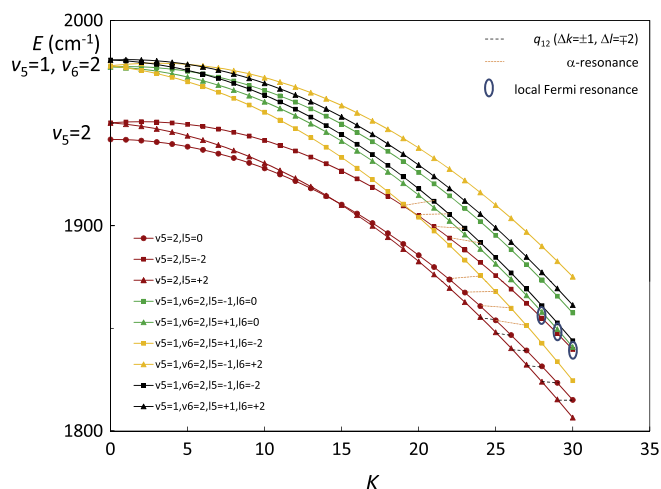


**Fig. 8.** The  $K$ -dependent part of the energy terms  $E = E_v + (C_v - B_v) K^2 - 2\sum_l (C_l^x l_x) K$  of the  $\nu_5 = 2$  and  $\nu_5 = 1$ ,  $\nu_6 = 2$  vibrational levels of DCF<sub>3</sub>. The local Fermi resonances are indicated by ellipses, the  $q_{12}$   $l$ -type resonance by black dashed lines, and the  $\alpha$ -resonances by orange dotted lines. (For interpretation of the references to color in this figure legend, the reader is referred to the web version of this article.)

constrained to the above-mentioned value, while  $f_{32}^{xxa}$  and  $f_{32}^{xxb}$  could be refined, together with the Coriolis terms  $f_{31}^{xa}$  and  $f_{31}^{xb}$ .

The vibrational diagonal molecular parameters of the  $\nu_5 = 2$  and  $\nu_5 = 1$ ,  $\nu_6 = 2$  levels are given in Table 2; those of the  $\nu_2 = \nu_5 = 1$  and  $\nu_2 = 1$ ,  $\nu_6 = 2$  levels are listed in Table 3. The inter-vibrational interaction parameters for both the  $\nu_5 = 2/\nu_5 = 1$ ,  $\nu_6 = 2$  and  $\nu_2 = \nu_5 = 1/\nu_2 = 1$ ,  $\nu_6 = 2$  level systems are in Table 4.

The details of the reproduction of the experimental data are available in the Supplementary material accompanying this paper (see Appendix B).

For the  $\nu_2 = \nu_5 = 1$  level, the fitted parameters generally show a good consistency with the parameters of the two fundamental levels. As in the case of the  $\nu_2 + \nu_3$  [2] and  $\nu_2 + \nu_6$  [6] combination

bands, the centrifugal distortion constants follow the rather anomalous values of the  $\nu_2 = 1$  fundamental level [2]. In the case of the  $\nu_2 = 1$  level, the higher  $\nu_4 = 1$  level was already identified as the most probable perturber, through a first-order  $x, y$  – Coriolis interaction. We can thus expect a similar coupling scheme between the  $\nu_2 = \nu_5 = 1$  level studied here and the higher  $\nu_4 = \nu_5 = 1$  ( $A_1 + A_2 + E$ ) level. However this latter level is likely to be involved in a Fermi resonance with five other levels [16,17]:  $2\nu_4/\nu_3 + \nu_4 + \nu_6/2\nu_3 + 2\nu_6/\nu_1/\nu_4 + \nu_5/\nu_3 + \nu_5 + \nu_6$ . As the interactions in this complex polyad are not fully understood yet, we preferred not including them explicitly in our model. This might explain the anomalous values of the centrifugal distortion constants of the  $\nu_2 = \nu_5 = 1$  level, which have to be thought of as fitting parameters rather than as having a physical meaning.

The accidental smallness of the  $q_{22}$   $l$ -type interaction parameter, already noticed for the  $\nu_5 = 1$  fundamental level, can be still noted for the  $\nu_2 = \nu_5 = 1$  combination level. The latter  $q_{22}$  value remains of the same order of magnitude as the former ( $\sim 10^{-5}$   $\text{cm}^{-1}$ ), even though it is more than twice greater in absolute value. We have to notice, however, an important difference between the  $q_{22}$  interaction parameters of the two above-mentioned states:  $q_{22}^{\nu_5=2}$  is positive, whereas  $q_{22}^{\nu_5=1}$  has a negative value. Indeed in the  $\nu_2 = \nu_5 = 1$  level, the  $k'l = +1$   $A_-$  sublevel lies above the  $A_+$  one; the relative position of the  $k'l = +1$  sublevels is interchanged with respect to that occurring in the  $\nu_5 = 1$  level.

This very subtle difference can be attributed to the different interaction patterns of  $\nu_5 = 1$  and  $\nu_2 = \nu_5 = 1$ . For the former the neglected interaction that contributes to the effective values of spectroscopic constants, including  $q_{22}^{\nu_5=1}$ , was the first-order Coriolis coupling with  $\nu_2 = 1$ , while for the  $\nu_2 = \nu_5 = 1$  level there are many more potential perturbing levels with smaller separation than that between  $\nu_5 = 1$  and  $\nu_2 = 1$ .

## 6. Conclusion

The current study represents a further step in the global understanding of the vibrational pattern of DCF<sub>3</sub> up to the highest fundamental vibration  $\nu_1$ , near  $2200 \text{ cm}^{-1}$ .

In this work, the  $v_5 = 2$  overtone levels were treated by considering their important anharmonic and Coriolis interactions with the neighboring ( $v_5 = 1$ ,  $v_6 = 2$ ) ‘dark’ levels. The reproduction of the experimental data is quantitative and results in very accurate molecular parameters.

For the  $v_2 = v_5 = 1$  combination level, only its interactions with the ( $v_2 = 1$ ,  $v_6 = 2$ ) ‘dark’ levels have been considered so far. The theoretical model already employed for the  $v_5/2v_6$  lower dyad [5] was thus extrapolated to the present case. It has been shown that the effects of neglected interactions with the complex vibrational polyad near  $2200 \text{ cm}^{-1}$  can be absorbed into effective values of the centrifugal distortion constants of the  $v_2 = v_5 = 1$  combination level. Moreover, this analysis agrees with the observed trends in the  $v_2 = 1$  level and provides a quantitative reproduction of all data included in the analysis.

## Acknowledgments

A. Predoi-Cross is grateful for financial support provided by NSERC. The experiments were carried out at the Canadian Light Source, which is supported by NSERC, NRC, CIHR, and the University of Saskatchewan.

## Appendix A. Definition of the matrix elements of the effective vibration–rotational Hamiltonian

### A.1. Diagonal matrix elements and intra-vibrational interactions

The diagonal matrix elements were defined conventionally as

$$E_{vr}(J, k) = E_v + B_{vj}(J+1) + (C_v - B_v)k^2 - D_v^j J^2 (J+1)^2 - D_{jk}^v J(J+1)k^2 - D_k^v k^4 + H_v^j J^3 (J+1)^3 + H_{jk}^v J^2 (J+1)^2 k^2 + H_{kj}^v J(J+1)k^4 + H_k^v k^6 + \left[ -2 \sum_t (C_{\zeta_t}^v)_{vt} + \sum_t \eta_{tj} J(J+1)l_t + \sum_t \eta_{tk} k^2 l_t + \sum_t \tau_{tj} J^2 (J+1)^2 l_t + \sum_t \tau_{tj} J(J+1)k^2 l_t + \sum_t \tau_{tk} k^4 l_t \right] k \quad (\text{A1})$$

In the z-Coriolis part of this expression, the summation over  $t$  in spans all degenerate modes which are excited in the overtone or combination states. In this place we use sometimes (as in Table 2) an ‘‘effective’’ value, approximately corresponding to  $-C_{\zeta_5}^v + 2C_{\zeta_6}^v$  and  $C_{\zeta_5}^v + 2C_{\zeta_6}^v$  for the sublevels  $v_5^j = 1^{\mp 1}$ ,  $v_6^j = 2^{\pm 2}$  and  $v_5^j = 1^{\pm 1}$ ,  $v_6^j = 2^{\pm 2}$ , respectively. The same approach is used for the expansion terms of the z-Coriolis operator. Obviously, the z-Coriolis part vanishes for the nondegenerate vibrational levels, i.e. the ground, the ( $v_5^j = 2^0$ ) and the ( $v_2 = 1$ ,  $v_6^j = 2^0$ ) states.

In the  $v_5 = 2$ ,  $v_2 = v_5 = 1$  and  $v_2 = 1$ ,  $v_6 = 2$  vibrational levels, the following  $q_{22}$  off-diagonal  $l$ -type matrix elements were taken into account

$$\langle v_t^{\pm 2}; J, k \pm 2 | \mathbf{H}_{22} + \mathbf{H}_{24} | v_t^{\pm 1}; J, k \rangle = [(v_t \mp l_t)(v_t \pm l_t + 2)]^{1/2} \{ q_{22} + f_{22}^j J(J+1) + f_{22}^k [k^2 + (k \pm 2)^2] \} F_2^{\pm}(J, k) \quad (\text{A2})$$

For the  $v_5 = 1$ ,  $v_6 = 2$  level, there are in fact two such operators, corresponding to  $\Delta l_5 = \pm 2$  and  $\Delta l_6 = \pm 2$  respectively (for details, see e.g. Ref. [14]).

The other off-diagonal  $l$ -type matrix elements considered in the  $v_5 = 2$  and  $v_2 = v_5 = 1$  vibrational levels were as follows

$$\langle v_t^{\pm 2}; J, k \mp 4 | \mathbf{H}_{24} | v_t^{\pm 1}; J, k \rangle = [(v_t \mp l_t)(v_t \pm l_t + 2)]^{1/2} f_{42}^{\mp} F_4^{\mp}(J, k) \quad (\text{A3})$$

$$\langle v_t^{\pm 2}; J, k \mp 1 | \mathbf{H}_{22} + \mathbf{H}_{24} | v_t^{\pm 1}; J, k \rangle = [(v_t \mp l_t)(v_t \pm l_t + 2)]^{1/2} \{ [q_{12} + f_{12}^j J(J+1)](2k \mp 1) + f_{12}^k [k^3 + (k \mp 1)^3] \} F_1^{\mp}(J, k) \quad (\text{A4})$$

$$\langle v_t^{\pm 2}; J, k \mp 1 | \mathbf{H}_{41} + \mathbf{H}_{43} | v_t^{\pm 1}; J, k \rangle = [(v_t \mp l_t)(v_t \pm l_t + 2)]^{1/2} \{ q_{12}^j + f_{12}^j J(J+1) + f_{12}^k [k^2 + (k \mp 1)^2] \} (2l_t \pm 2) F_1^{\mp}(J, k) \quad (\text{A5})$$

Matrix elements of the  $\Delta k = \pm 3$  operator were written as

$$\langle v_t^{\pm 1}; J, k \pm 3 | \mathbf{H}_{23} + \mathbf{H}_{25} | v_t^{\pm 1}; J, k \rangle = [d_t + d_t^j J(J+1)] l_t F_3^{\pm}(J, k) \quad (\text{A6})$$

and the matrix elements of the  $\Delta k = \pm 6$  operator

$$\langle v_t^{\pm 1}; J, k \pm 6 | \mathbf{H}_{06} + \mathbf{H}_{08} | v_t^{\pm 1}; J, k \rangle = [h_3 + h_3^j J(J+1)] F_6^{\pm}(J, k) \quad (\text{A7})$$

### A.2. Inter-vibrational interactions

#### 1. The $2v_5/v_5 + 2v_6$ system

A rovibrational ket is denoted throughout this subsection by  $|v_t^{\pm 1}, v_{t'}^{\pm 1}; J, k\rangle$ , where  $t = 5$  and  $t' = 6$ .

- Matrix elements of the Fermi operator

$$\langle 2^0, 0^0; J, k | \mathbf{H}_{30} | 1^{\pm 1}, 2^{\pm 2}; J, k \rangle = \frac{3}{4} \sqrt{2} k_{ta2t'a} \quad (\text{A8})$$

$$\langle 2^{\mp 2}, 0^0; J, k | \mathbf{H}_{30} | 1^{\mp 1}, 2^{\pm 2}; J, k \rangle = \frac{3}{2} k_{ta2t'a} \quad (\text{A9})$$

- Matrix elements of the Coriolis operators  $\mathbf{H}_{31}^{xa}$  and  $\mathbf{H}_{31}^{xb}$

$$\langle 2^{\pm 2}, 0^0; J, k \pm 1 | \mathbf{H}_{31}^{xa} | 1^{\pm 1}, 2^0; J, k \rangle = \pm f_{31}^{xa} \sqrt{2} F_1^{\pm}(J, k) \quad (\text{A10})$$

$$\langle 2^0, 0^0; J, k \pm 1 | \mathbf{H}_{31}^{xa} | 1^{\mp 1}, 2^0; J, k \rangle = \pm f_{31}^{xa} F_1^{\pm}(J, k) \quad (\text{A11})$$

$$\langle 2^0, 0^0; J, k \pm 1 | \mathbf{H}_{31}^{xb} | 1^{\pm 1}, 2^{\mp 2}; J, k \rangle = \pm f_{31}^{xb} \sqrt{2} F_1^{\pm}(J, k) \quad (\text{A12})$$

$$\langle 2^{\mp 2}, 0^0; J, k \pm 1 | \mathbf{H}_{31}^{xb} | 1^{\mp 1}, 2^{\mp 2}; J, k \rangle = \pm 2 f_{31}^{xb} F_1^{\pm}(J, k) \quad (\text{A13})$$

- Matrix elements of the  $\alpha$ -resonance operators  $\mathbf{H}_{32}^{xxa}$  and  $\mathbf{H}_{32}^{xxb}$

$$\langle 2^{\pm 2}, 0^0; J, k \mp 2 | \mathbf{H}_{32}^{xxa} | 1^{\pm 1}, 2^0; J, k \rangle = f_{32}^{xxa} \sqrt{2} F_2^{\mp}(J, k) \quad (\text{A14})$$

$$\langle 2^0, 0^0; J, k \mp 2 | \mathbf{H}_{32}^{xxa} | 1^{\mp 1}, 2^0; J, k \rangle = f_{32}^{xxa} F_2^{\mp}(J, k) \quad (\text{A15})$$

$$\langle 2^0, 0^0; J, k \mp 2 | \mathbf{H}_{32}^{xxb} | 1^{\pm 1}, 2^{\mp 2}; J, k \rangle = f_{32}^{xxb} \sqrt{2} F_2^{\mp}(J, k) \quad (\text{A16})$$

$$\langle 2^{\mp 2}, 0^0; J, k \mp 2 | \mathbf{H}_{32}^{xxb} | 1^{\mp 1}, 2^{\mp 2}; J, k \rangle = 2 f_{32}^{xxb} F_2^{\mp}(J, k) \quad (\text{A17})$$

- Matrix element of the higher-order anharmonic resonance

$$\langle 2^{\mp 2}, 0^0; J, k | \mathbf{H}_{50} | 1^{\pm 1}, 2^0; J, k \rangle = W_{55566} \quad (\text{A18})$$

#### 2. The $v_2 + v_5/v_2 + 2v_6$ system

The matrix elements describing the inter-vibrational interactions correspond to those already given in Ref. [5] for the  $v_5/2v_6$  lower system. The theoretical model is indeed the same, and moreover, adding one vibrational quantum of the nondegenerate vibration  $v_2$  does not change the vibrational coefficients of the inter-vibrational matrix elements.

The notation of the matrix elements of the rotational shifting operators was taken as

$$F_n^\pm(J, k) = \prod_{i=1}^n [J(J+1) - (k \pm i \mp 1)(k \pm i)]^{1/2} \quad (\text{A19})$$

## Appendix B. Supplementary material

Supplementary data for this article are available on Science Direct ([www.sciencedirect.com](http://www.sciencedirect.com)) and as part of the Ohio State University Molecular Spectroscopy Archives ([http://library.osu.edu/sites/msa/jmsa\\_hp.htm](http://library.osu.edu/sites/msa/jmsa_hp.htm)). Supplementary data associated with this article can be found, in the online version, at <http://dx.doi.org/10.1016/j.jms.2014.09.002>.

## References

- [1] H.-R. Dübal, M. Lewerenz, M. Quack, *J. Chem. Phys.* 85 (1986) 34–39.
- [2] P. Pracna, Š. Urban, F. Kolář, J. Cosléou, J. Demaison, P. Papelewski, H. Bürger, *J. Mol. Struct.* 517–518 (2000) 119–126.
- [3] P. Pracna, A. Ceausu-Velcescu, A. Predoi-Cross, Š. Urban, *J. Mol. Spectrosc.* 259 (2010) 1–10.
- [4] P. Pracna, A. Ceausu-Velcescu, H. Bürger, *J. Mol. Spectrosc.* 250 (2008) 59–69.
- [5] A. Ceausu-Velcescu, P. Pracna, A. Predoi-Cross, *J. Mol. Spectrosc.* 267 (2011) 150–157.
- [6] P. Pracna, T. Prętkowski, W. Łodyga, M. Kręglewski, *J. Mol. Spectrosc.* 275 (2012) 31–34.
- [7] A. Ceausu-Velcescu, P. Pracna, *J. Mol. Spectrosc.* 275 (2012) 41–47.
- [8] A. Ceausu-Velcescu, P. Pracna, *J. Mol. Spectrosc.* 295 (2014) 31–36.
- [9] A. Ceausu-Velcescu, H. Bürger, G. Graner, *J. Mol. Spectrosc.* 220 (2003) 298–305.
- [10] A.S. Pine, J.M. Plíva, *J. Mol. Spectrosc.* 130 (1988) 431–444.
- [11] A.S. Pine, G.T. Fraser, J.M. Plíva, *J. Chem. Phys.* 89 (1988) 2720–2728.
- [12] W. Łodyga, M. Kręglewski, P. Pracna, Š. Urban, *J. Mol. Spectrosc.* 243 (2007) 182–188.
- [13] G. Amat, H.H. Nielsen, *J. Chem. Phys.* 36 (1962) 1859–1865.
- [14] P. Pracna, J. Demaison, G. Włodarczak, A.G. Lesarri, G. Graner, *J. Mol. Spectrosc.* 177 (1996) 124–133; P. Pracna, K. Sarka, J. Demaison, J. Cosléou, F. Herlemont, M. Khelkhal, H. Fichoux, D. Papoušek, M. Papelewski, H. Bürger, *J. Mol. Spectrosc.* 184 (1997) 93–105.
- [15] U. Wötzel, H. Mäder, H. Harder, P. Pracna, K. Sarka, *Chem. Phys.* 312 (2005) 159–167.
- [16] G. Klatt, A. Willetts, N.C. Handy, R. Tarroni, P. Palmieri, *J. Mol. Spectrosc.* 176 (1996) 64–74.
- [17] J. Breidung, J. Cosléou, J. Demaison, K. Sarka, W. Thiel, *Mol. Phys.* 102 (2004) 1827–1841.